SPANDIDOS PUBLICATIONS

INTERNATIONAL JOURNAL OF MOLECULAR MEDICINE 52: 99, 2023

UCHL1 alleviates apoptosis in chondrocytes via upregulation of HIF-1α-mediated mitophagy

QIQIAN YAN[1,2], SHANWEI SHI[1,2], YANG GE[1,2], SHUANGQUAN WAN[1,2], MINGFEI LI[1,2] and MAOQUAN LI[1,2]

[1]Stomatological Hospital, School of Stomatology, Southern Medical University, Guangzhou, Guangdong 510280; [2]Guangdong Academy of Stomatology, Guangzhou, Guangdong 510180, P.R. China

Received May 18, 2023; Accepted August 16, 2023

DOI: 10.3892/ijmm.2023.5302

Abstract. Stem cell-based tissue engineering has shown significant potential for rapid restoration of injured cartilage tissues. Stem cells frequently undergo apoptosis because of the prevalence of oxidative stress and inflammation in the microenvironment at the sites of injury. Our previous study demonstrated that stabilization of hypoxia-inducible factor 1α (HIF-1α) is key to resisting apoptosis in chondrocytes. Recently, it was reported that Ubiquitin C-terminal hydrolase L1 (UCHL1) can stabilize HIF-1α by abrogating the ubiquitination process. However, the effect of UCHL1 on apoptosis in chondrocytes remains unclear. Herein, adipose-derived stem cells were differentiated into chondrocytes. Next, the CRISPR activation (CRISPRa) system, LDN-57444 (LDM; a specific inhibitor for UCHL1), KC7F2 (a specific inhibitor for HIF-1α), and 3-methyladenine (a specific inhibitor for mitophagy) were used to activate or block UCHL1, HIF-1α, and mitophagy. Mitophagy, apoptosis, and mitochondrial function in chondrocytes were detected using immunofluorescence, TUNEL staining, and flow cytometry. Moreover, the oxygen consumption rate of chondrocytes was measured using the Seahorse XF 96 Extracellular Flux Analyzer. UCHL1 expression was increased in hypoxia, which in turn regulated mitophagy and apoptosis in the chondrocytes. Further studies revealed that UCHL1 mediated hypoxia-regulated mitophagy in the chondrocytes. The CRISPRa module was utilized to activate UCHL1 effectively for 7 days; endogenous activation of UCHL1 accelerated mitophagy, inhibited apoptosis, and maintained mitochondrial function in the chondrocytes, which was mediated by HIF-1α. Taken together, UCHL1 could block apoptosis in chondrocytes via upregulation of HIF-1α-mediated mitophagy and maintain mitochondrial function. These results indicate the potential of UCHL1 activation using the CRISPRa system for the regeneration of cartilage tissue.

Correspondence to: Dr Maoquan Li, Stomatological Hospital, School of Stomatology, Southern Medical University, 366 South Jiangnan Avenue, Haizhu, Guangzhou, Guangdong 510280, P.R. China
E-mail: maoquan_li@qq.com

Abbreviations: 3-MA, 3-Methyladenine; ROS, reactive oxygen species; HIF-1α, hypoxia-inducible factor 1α; PHD2, prolyl hydroxylase 2; VHL, von hippel-lindau; UCHL1, Ubiquitin C-terminal hydrolase-L1; CRISPRa, CRISPR activation; ADSCs, adipose-derived stem cells; FCM, flow cytometry; ALP, alkaline phosphatase; dpt, day post-transduction; MMP, Mitochondrial membrane potential; DCFH-DA, dichloro-dihydro-fluorescein diacetate; OCR, oxygen consumption rate; FCCP, fluoromethoxy carbonyl cyanide phenylhydrazone; Sa, Staphylococcus aureus; CBP, CREB-binding protein; DMOG, dimethyloxalylglycine

Key words: UCHL1, HIF-1α, ADSCs, mitophagy, apoptosis, CRISPR

Introduction

Cartilage defects caused by trauma, congenital malformations, or oncological resection are often devastating and cannot be cured because of the intrinsically low regenerative capacity of cartilage tissues (1). Autologous cartilage grafting as well as modified operations, such as cartilage transplantation combined with flap transfer have been developed to treat nasal, auricular, and tracheal defects (2-4). However, cartilage tissue is inevitably wasted during graft carving, and ensuring an accurate shape of a graft may require extensive engraving techniques (5). Tissue engineering offers the possibility of replacing damaged chondral tissue as an alternative to cartilage grafting. In this regard, stem cell-based tissue engineering approaches have recently exhibited significant potential for rapidly restoring injured cartilage tissues (6). For example, stem cells that are transplanted successfully can differentiate into chondrocytes for functional restoration (7). However, stem cells frequently undergo apoptosis because of the prevalence of oxidative stress and inflammation in the microenvironment of injured sites (8). Hence, there is an urgent need to find an effective method to abrogate apoptosis as survival in hostile conditions is a prerequisite for cells to perform various physiological functions.

Mitochondria are one of the most complex and important organelles present in eukaryotes, which convert organic matter into carbon dioxide and water through redox reactions (9). Mitochondrial dysfunction leads to the irregular transfer of electrons generated by redox reactions to oxygen, water, or their intermediate states, thus forming large quantities of reactive oxygen species (ROS), eventually leading to cell death (10,11). Mitophagy, a special form of autophagy, is a

process of selective removal of excess or damaged mitochondria that plays an important role in maintaining mitochondrial homeostasis and regulating the number of mitochondria in cells (12,13). Under various conditions of cellular stress, including low oxygen conditions, oxidative stress, and high glucose levels, mitophagy can be activated; the upregulated mitophagy can promote cell survival by removing damaged mitochondria (14). Recently, there has been increasing evidence that induction of mitophagy plays a crucial role in preventing chondrocyte apoptosis (15-17).

In healthy cartilage, chondrocytes exist in relatively low oxygen conditions, in which hypoxia-inducible factor 1α (HIF-1α) plays a vital role in regulating chondrogenesis by directing the differentiation of progenitor cells and maintaining appropriate extracellular matrix production (18). Our previous study showed that chondrocytes are well adapted to hypoxia and produce a more functional extracellular matrix in low-oxygen environments *in vitro* (19). This effect is reversed in the presence of high oxygen concentrations, as HIF-1α is degraded in high oxygen conditions, which in turn promotes further apoptosis of chondrocytes (20). Therefore, the stabilization of HIF-1α is key to the survival of chondrocytes. The prolyl hydroxylase 2 (PHD2)-von Hippel Lindau (VHL) signaling cascade is central to the regulation of HIF-1α (21). Under physiological conditions, PHD2 hydroxylate residues are present on the oxygen-dependent degradation domain of HIF-1α; VHL, as a part of the E3 ubiquitin ligase complex, recognizes the motifs of the hydroxylated residues, resulting in rapid degradation of HIF-1α. However, PHD2 is less active during hypoxia, which leads to cytosolic accumulation and nuclear translocation of HIF-1α, where, together with transcriptional cofactors, it activates the expression of its target genes in the HIF complex, such as BNIP3, an essential molecule for mitophagy (22,23). It has been shown to stimulate chondrogenesis of progenitor or stem cells by decreasing the oxygen pressure locally within a biomaterial using various molecules or simply by limiting oxygen diffusion (24,25).

However, regulating oxygen itself may not be ideal because hypoxia is also known to cause oxidative stress, negatively impact cell growth and viability, and boost potentially undesirable effects on cell metabolism (26). Recently, it was demonstrated that Ubiquitin C-terminal hydrolase-L1 (UCHL1) protects against ischemic heart injury by increasing the stability of HIF-1α (27). Moreover, UCHL1 was reported to abrogate VHL-mediated ubiquitination of HIF-1α (28). However, the effect of UCHL1, with its function of binding and stabilizing HIF-1α, on apoptosis in chondrocytes is unclear.

In the present study, adipose-derived stem cells (ADSCs) were utilized to differentiate into chondrocytes. Next, a series of *in vitro* experiments were performed to assess mitophagy, apoptosis, and mitochondrial function in the chondrocytes. Moreover, the CRISPR activation (CRISPRa) system was used to activate endogenous UCHL1 in chondrocytes. The results revealed that activation of UCHL1 using CRISPRa inhibited apoptosis and maintained mitochondrial function, resulting in the survival of chondrocytes. This provides a theoretical basis for tissue engineering strategies that can be used for the treatment of cartilage defects.

Materials and methods

Cell culture and reagents. ADSCs were purchased from Procell Life Science Technology Co., Ltd. (cat. no. CP-R147) and were cultured in α-MEM medium (HyClone; Cytiva) supplemented with 10% (v/v) FBS (HyClone; Cytiva), 100 U/ml penicillin, and 100 U/ml streptomycin at 37˚C with 5% CO_2 in a humidified chamber. The cells were passaged 3-5 times and used for subsequent experiments. To induce hypoxia in cell cultures, the cells were subjected to a hypoxic environment using a specialized incubator with an oxygen concentration of 1% for a duration of 24 h. In contrast, the control group was exposed to a normoxic environment maintaining a regular oxygen concentration of 20%.

Insect cells (Sf-9) were purchased from the American Type Culture Collection Cell Bank for baculovirus generation and were cultured in TNM-FH medium (HyClone; Cytiva) supplemented with 10% FBS. Stock solutions of LDN (MilliporeSigma; cat. no. L4170) and KC7F2 (MilliporeSigma; cat. no. SML1043) were prepared in DMSO (10 mM and 30 μM, respectively) obtained from the Beyotime Institute of Biotechnology. 3-Methyladenine (3-MA, MilliporeSigma; cat. no. M9281) was prepared in DMEM solution (5 mM). In the present study, cells were treated with the corresponding blocker for 2 h, after which they were subsequently subjected to relevant tests.

Characterization of ADSCs. To identify the phenotypes of ADSCs, flow cytometry (FCM, CytoFLEX S; Beckman Coulter Life Sciences) was used to screen for surface markers against CD29 (0.2 mg/ml; cat. no. 562153), CD34 (0.2 mg/ml; cat. no. 560233), CD44 (0.5 mg/ml; cat. no. 550974), CD45 (0.2 mg/ml; cat. no. 561586), CD73 (0.5 mg/ml; cat. no. 551123), and CD90 (0.2 mg/ml; cat. no. 561409), which were all purchased from BD Biosciences; Becton, Dickinson and Company. Briefly, the cells were collected, washed and then suspended in flow cytometry staining buffer (cat. no. 554656; BD Biosciences) containing the aforementioned antibodies at 25˚C for 30 min before being subjected to flow cytometric analysis. Acquired data were analyzed using FlowJo software (v.10.8.1; FlowJo, LLC). ADSCs were induced to differentiate into chondrocytes, osteocytes, and adipocytes using chondrogenic, osteogenic, and adipogenic media as described in previous studies (29,30). After 21 days of induction by the chondrogenic medium supplemented with 1x insulin-transferrin-selenium (Corning, Inc.), ADSCs were fixed at 25˚C with 4% (w/v) paraformaldehyde for 15 min and then stained for 30 min at 4˚C with 0.5% alcian blue dye (MilliporeSigma) in 1 mol/l HCl to detect the extracellular matrix of chondrocytes. For osteogenic differentiation, the cells were cultured in an induction medium supplemented with 10 nM dexamethasone (Beyotime Institute of Biotechnology), 10 mM β-glycerophosphate (Beyotime Institute of Biotechnology), and 50 μg/ml L-ascorbic acid (Beyotime Institute of Biotechnology) for 7 days and stained using an alkaline phosphatase (ALP) assay kit according to the manufacturer's protocol (Beyotime Institute of Biotechnology; cat. no. P0321S); while after 14 days the cells were stained using the Alizarin Red S Staining kit according to the manufacturer's protocol (Beyotime Institute

of Biotechnology; cat. no. C0148S). For adipogenic induction, cells were subjected to Oil Red O staining (Beyotime Institute of Biotechnology; cat. no. C0157S) after 21 days of induction in the adipogenic medium supplemented with 10 μM dexamethasone (Beyotime Institute of Biotechnology), 25 mM 3-isobutyl-1-methylxanthine (MilliporeSigma), 2 μM rosiglitazone (MilliporeSigma), and 1 μg/ml insulin (Beyotime Institute of Biotechnology).

Construction and preparation of baculovirus vectors. The construction of a viral vector (designated as pBac-Sa-con) was divided into four steps. All primers used for the construction of the virus are listed in Table SI. First, a DNA fragment composed of tandem recombination sites (KpnI-loxP-NheI-XhoI-NotI-PacI-EcoRI-BamHI-loxP-HindIII) was chemically synthesized by Detai Bioscience, Inc. (the full sequence is listed in Fig. S1) and subcloned into pFastBac Dual (Gibco; Thermo Fisher Scientific, Inc.) using KpnI/HindIII (Beyotime Institute of Biotechnology) digestion to yield the vector, pL. Second, the CMV enhancer-rEF-1α promoter fragment was PCR-amplified from pVITRO1-neo-mcs (Invivogen; cat. no. pvitro1-nmcs) and subcloned into pL between the XhoI and NotI sites to generate the vector, pLE. Third, the cDNA of a woodchuck hepatitis virus post-transcriptional regulatory element (WPRE), which enhances mRNA stability, was amplified from pENN.AAV.hSyn.Cre.WPRE.hGH (Addgene; cat. no. 105553) and subcloned into pLE using EcoRI/BamHI (Beyotime Institute of Biotechnology) to generate the vector, pLEW. Finally, a Sa-deadCas9-VPR (Sa-dCas9-VPR) fragment was PCR-amplified from SadCas9VPR (Addgene, cat. no. 188514) and inserted into pLEW between the PacI and EcoRI sites to yield pBac-Sa-con.

Single guide (sg)RNA cassettes of Sa-dCas9 were synthesized using sequences of pGL3-U6-sgRNA-PGK-puromycin (Addgene; cat. no. 51133), which contains a human U6 (hU6) promoter, a spacer sequence, and a sgRNA scaffold. Spacer sequences targeting UCHL1 with the highest targeting specificity scores (5'-ACCGGTGAGACCACCACCAGATTAGCTCACCGGCGAGTGGTCTCAGTTTG-3') were designed using a guide RNA design tool (www.benchling.com). The resulting sgRNA sequences were subcloned into pBac-Sa-con to yield pBac-Sa-UCHL1 using the NheI reagent (Beyotime Institute of Biotechnology). The donor plasmids pBac-Sa-con and pBac-Sa-UCHL1 were used to generate baculoviruses Bac-Sa-con and Bac-Sa-UCHL1, respectively, using the Bac-To-Bac® system (Invitrogen; Thermo Fisher Scientific, Inc.). The recombinant BV vectors were amplified by infecting Sf-9 insect cells and titrated using the end-point dilution method (31).

Baculovirus transduction. For transduction, cells cultured overnight were washed twice with PBS before being transduced with Bac-Sa-con and Bac-Sa-UCHL1. Depending on the multiplicity of infection (MOI, pfu/cell) and virus titer, a certain volume of the virus supernatant was mixed with $NaHCO_3$-free DMEM at a volumetric ratio of 1:4 and added to the cells. The cells were gently shaken on a rocking plate at 25°C for 6 h, after which the solution was replaced with α-MEM medium containing 3 mM sodium butyrate (MilliporeSigma), and the cells were further cultured. At day 1 post-transduction (dpt), the medium was replaced with either fresh α-MEM or chondroinductive medium. The chondroinductive medium was replaced every 2-3 days until performing *in vitro* analysis.

RNA extraction and reverse transcription-quantitative (RT-q) PCR. Total RNA from ADSCs or chondrocytes in different groups was measured using a Nanodrop 2000 spectrophotometer (Thermo Fisher Scientific, Inc.) and reverse transcribed to cDNA using a PrimeScript™ RT Master Mix according to the manufacturer's protocol (Takara Bio, Inc.; cat. no. RR047A). qPCR was performed using the PrimeScript RT-PCR kit (Takara Bio, Inc.; cat. no. RR820A), and the primers used are listed in Table SII. Relative mRNA expression of target genes was calculated using the $2^{-\Delta\Delta Cq}$ method (32). The thermocycling conditions were: Initial denaturation for 30 sec at 95°C; followed by 40 cycles of 95°C for 5 sec, 60°C for 30 sec, and 95°C for 5 sec; melting at 65°C for 60 sec and 97°C for 1 sec; and cooling at 50°C for 30 sec. The experiments were performed in triplicates and repeated three times.

Immunofluorescence (IF) staining. To detect the expression of UCHL1 in hypoxia and HIF-1α after activation of UCHL1, chondrocytes were stained with DAPI (Beyotime Institute of Biotechnology; cat. no. C1005) at 25°C for 5 min and simultaneously stained with antibodies against UCHL1 (1:200; Cell Signaling Technology; cat. no. 13179) or HIF-1α (1:100; Cell Signaling Technology; cat. no. 48085) at a temperature of 37°C for 1 h. To verify the levels of mitophagy in different groups, chondrocytes were stained with DAPI at 25°C for 5 min and simultaneously stained with antibodies against LC3B (1:200, Cell Signaling Technology, cat. no. 3868) and Tom20 (1:200; Cell Signaling Technology, cat. no. 42406) at 37°C for 1 h. Next, the cells were stained with the corresponding secondary antibodies (Alexa Fluor® 488- or 594-conjugated goat anti-rabbit or anti-mouse IgG, all 1:1,000, Abcam; cat. nos. ab150077, ab150113, ab150080, and ab150116) at 37°C for 1 h. Images were obtained using a laser scanning confocal microscope (magnification, x400; LSCM, Zeiss GmbH, cat. no. LSM780). In addition, the fluorescence intensity was measured using ImageJ version 2.1 (National Institutes of Health).

TUNEL staining. Damaged DNA was detected using a TUNEL Cell Apoptosis Detection Kit (Beyotime Institute of Biotechnology; cat. no. C1088). Chondrocytes were fixed and stained with TUNEL test solution for 30 min at 37°C according to the manufacturer's instructions, and the nuclei were stained with DAPI at 25°C for 5 min. A total of three fields of view were randomly selected and captured to count the number of TUNEL-positive cells.

Apoptosis. The Annexin V-APC Apoptosis Detection Kit (BioGems; cat. no. 62700-80) was used to determine the apoptotic ratio, according to the manufacturer's instructions. Briefly, chondrocytes were washed twice with Cell Staining Buffer and resuspended in Annexin V-Binding Buffer at a concentration of $1x10^7$ cells/ml. A total of 100 μl cell suspension was transferred to a 5 ml test tube, 5 μl APC Annexin V and 5 μl 7-AAD Viability Staining Solution were added in this order, and the cells were gently vortexed and incubated

for 15 min at 25˚C in the dark, and then 400 μl Annexin V Binding Buffer was added to each tube. The apoptosis ratio of chondrocytes was analyzed using FCM.

Mitochondrial membrane potential (MMP). A mitochondrial membrane potential assay kit with JC-1 (Beyotime Institute of Biotechnology; cat. no. C2003S) was used to assess the MMP. Chondrocytes were incubated with JC-1 (5 μM) for 30 min and DAPI for 5 min at 37˚C, then washed three times with PBS and observed using LSCM (magnification, x400).

The MMP was detected using MitoTracker Red CMXRos (Beyotime Institute of Biotechnology; cat. no. C1035). Chondrocytes were incubated with 50 nM Mito-tracker probes for 30 min at 37˚C according to the manufacturer's instructions. After staining with DAPI at 25˚C for 5 min, the cells were washed thrice with PBS, and images were captured using LSCM (magnification, x400).

Measurement of mitochondrial and intracellular ROS. Mito-SOX Red dye (Invitrogen; Thermo Fisher Scientific, Inc.; cat. no. M36008) was used to assess mitochondrial ROS levels. Chondrocytes from different groups were incubated with Mito-Sox Red dye (5 μM) for 30 min at 37˚C and stained with DAPI. The cells were then washed twice with PBS and observed using LSCM (magnification, x400).

Intracellular ROS was detected using the ROS Assay kit (Beyotime Institute of Biotechnology; cat. no. S0033M). After adding the dichloro-dihydro-fluorescein diacetate (DCFH-DA) probe at a final concentration of 10 μM, chondrocytes were incubated in the dark for 30 min at 37˚C and then stained with DAPI. Images were captured using LSCM (magnification, x400).

Cell proliferation. Chondrocyte growth was analyzed using a CCK-8 cell viability kit (Dojindo Molecular Technologies, Inc. Molecular Technologies, Inc.; cat. no. CK04-11). Briefly, cells were seeded into 96-well plates, and DMEM containing different concentrations of LDN was added for 1, 3, 5, or 7 days. CCK-8 reagent (10 μl) was added to each well and the plates were incubated at 37˚C for 2 h. The absorbance of the supernatant was measured at 450 nm using a microplate reader (Thermo Fisher Scientific, Inc.).

Seahorse metabolic flux analysis. The oxygen consumption rate (OCR) was measured using the Seahorse XF 96 Extracellular Flux Analyzer (Seahorse Bioscience; Agilent Technologies, Inc.) with the Agilent Seahorse XF Cell Mito Stress Test kit (Seahorse Bioscience; Agilent Technologies, Inc.; cat. no. 103015-100). Briefly, chondrocytes ($2x10^4$ cells/well) were seeded in a Seahorse XF 96-well cell culture plate. The loaded sensor cartridge with the utility plate was placed in the instrument for calibration, and oligomycin (1.5 μM), fluoromethoxy carbonyl cyanide phenylhydrazone (FCCP, 1.5 μM), rotenone, and antimycin A (1.25 μM) were sequentially added to each well after 20-, 40-, and 60-min. OCR data were assessed using the Seahorse XF-96 Wave software version 2.6 (Seahorse Bioscience; Agilent Technologies, Inc.).

Statistical analysis. Data are presented as mean ± SD of at least three independent experimental repeats. Following Shapiro-Wilk tests for assessment of normality and Levene's test for equality of variance, a paired Student's t-test was used to assess the differences between the control and test groups. One- and two-way ANOVA followed by a SNK post hoc test were used to analyze the differences in CCK-8 assays, quantitative analysis of LC3B, TUNEL staining, Cell apoptosis, and MMP between multiple groups after treatment with LDN, CRISPRa, KC7F2, or 3-MA. $P<0.05$ was considered to indicate a statistically significant difference.

Results

UCHL1 expression is increased under hypoxic conditions. ADSCs exhibited typical spindle and elongated fibroblast-like morphology (Fig. 1A). Mesenchymal stem cell markers (such as CD29, CD44, and CD90) and the pluripotent marker CD73 were highly expressed, whereas CD34 and CD45 (hematopoietic cell antigen) were undetectable (Fig. 1B). Alcian blue staining was used to demonstrate the chondrogenic differentiation ability of ADSCs, which was also evidenced by upregulation of chondrogenesis-related markers such as aggrecan, SOX9, and COL2A1 (Fig. 1C and D). The osteogenic differentiation ability of ADSCs was confirmed by the strong ALP and Alizarin Red staining as well as by upregulation of osteogenesis-related markers, such as RUNX2, ALP, and COL1 (Fig. 1E-G). Furthermore, Oil red O staining revealed differentiation of adipocytes (Fig. 1H). These results verified the potential of ADSCs to differentiate into multiple types of cells.

To investigate the effects of UCHL1 on apoptosis in chondrocytes, the chondrocytes differentiated from ADSCs were used for subsequent experiments. The IF staining results indicated that the levels of UCHL1 were enhanced under hypoxic conditions (Fig. 1I).

Hypoxia regulates mitophagy and apoptosis in chondrocytes. The results of IF staining indicated that the protein levels of LC3B increased under hypoxic conditions (Fig. 2A and B). To detect apoptosis, TUNEL assays and FCM were performed, and the results demonstrated that hypoxia reduced apoptosis (Fig. 2C-F). As a fluorescent probe used to detect MMP, the transformation of fluorescence of JC-1 from red to green fluorescence is an early indicator of apoptosis. The results of JC-1 staining also revealed that hypoxia inhibited apoptosis by increasing MMP levels (Fig. 2G). IF staining with MitoTracker Red revealed that MMP levels were also increased under hypoxic conditions (Fig. 2H and I). In addition, mitochondrial and intracellular ROS levels were significantly increased under hypoxic conditions (Fig. 2J-M).

UCHL1 mediates the mitophagy regulated by hypoxia in chondrocytes. To further confirm whether UCHL1 plays a role in hypoxia-induced mitophagy, chondrocytes were treated with LDN, a specific UCHL1 inhibitor. LDN was not cytotoxic to chondrocytes at 0, 1, 2, 4, and 8 μM concentrations after treatment for 1, 3, 5, and 7 days as observed using CCK-8 assays. However, the proliferation of the cells was significantly inhibited when treated with 16 μM LDN for 5 days (Fig. 3A). Thus, 8 μM LDN was utilized for 1 day in subsequent experiments. The increase in LC3B expression under hypoxic conditions was reversed by LDN treatment (Fig. 3B and C).

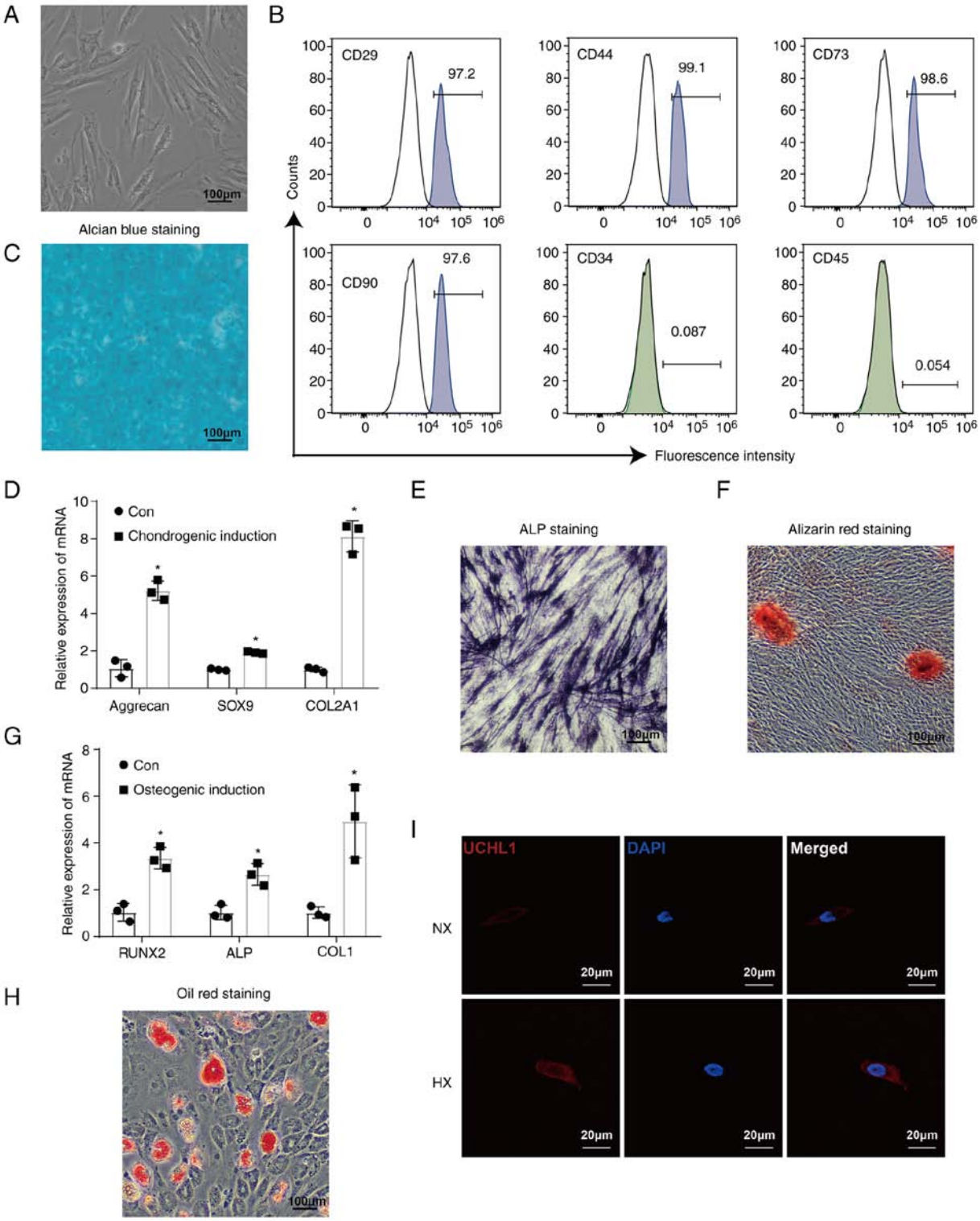

Figure 1. UCHL1 expression is increased under hypoxic conditions. (A) Images of ADSCs observed under a microscope (magnification, x40). (B) Mesenchymal stem cell antigens (CD29, CD44, CD73, and CD90) and hematopoietic cell antigens (CD34 and CD45). expressed in ADSCs were detected by flow cytometry. (C) Alcian blue staining of ADSCs after 21 days of chondrogenic induction (magnification, x40). (D) mRNA expression of chondrogenic markers Aggrecan, SOX9, and COL2A1 after 14 days of chondrogenic induction, as analyzed. (E) ALP staining of ADSCs after 7 days of osteogenic induction (magnification, x40). (F) Alizarin red staining of ADSCs after 14 days of osteogenic induction (magnification, x40). (G) mRNA expression of chondrogenic markers RUNX2, ALP, and COL1 after 14 days of osteogenic induction. (H) Oil red O staining of ADSCs after 21 days of adipogenic induction (magnification, x40). (I) Immunofluorescence staining of UCHL1 (magnification, x400). *P<0.05 vs. Con. NX, normoxia; HX, hypoxia; Con, control group; UCHL1, Ubiquitin C-terminal hydrolase-L1; ADSCs, adipose-derived stem cells; ALP, alkaline phosphatase.

The proportion of apoptotic cells, which had decreased under hypoxic conditions, increased when UCHL1 was inhibited (Fig. 3D-G). The increase in MMP observed under hypoxic conditions was also reversed by LDN (Fig. 3H-J). These results suggest that UCHL1 mediates mitophagy and apoptosis regulated by hypoxia in chondrocytes.

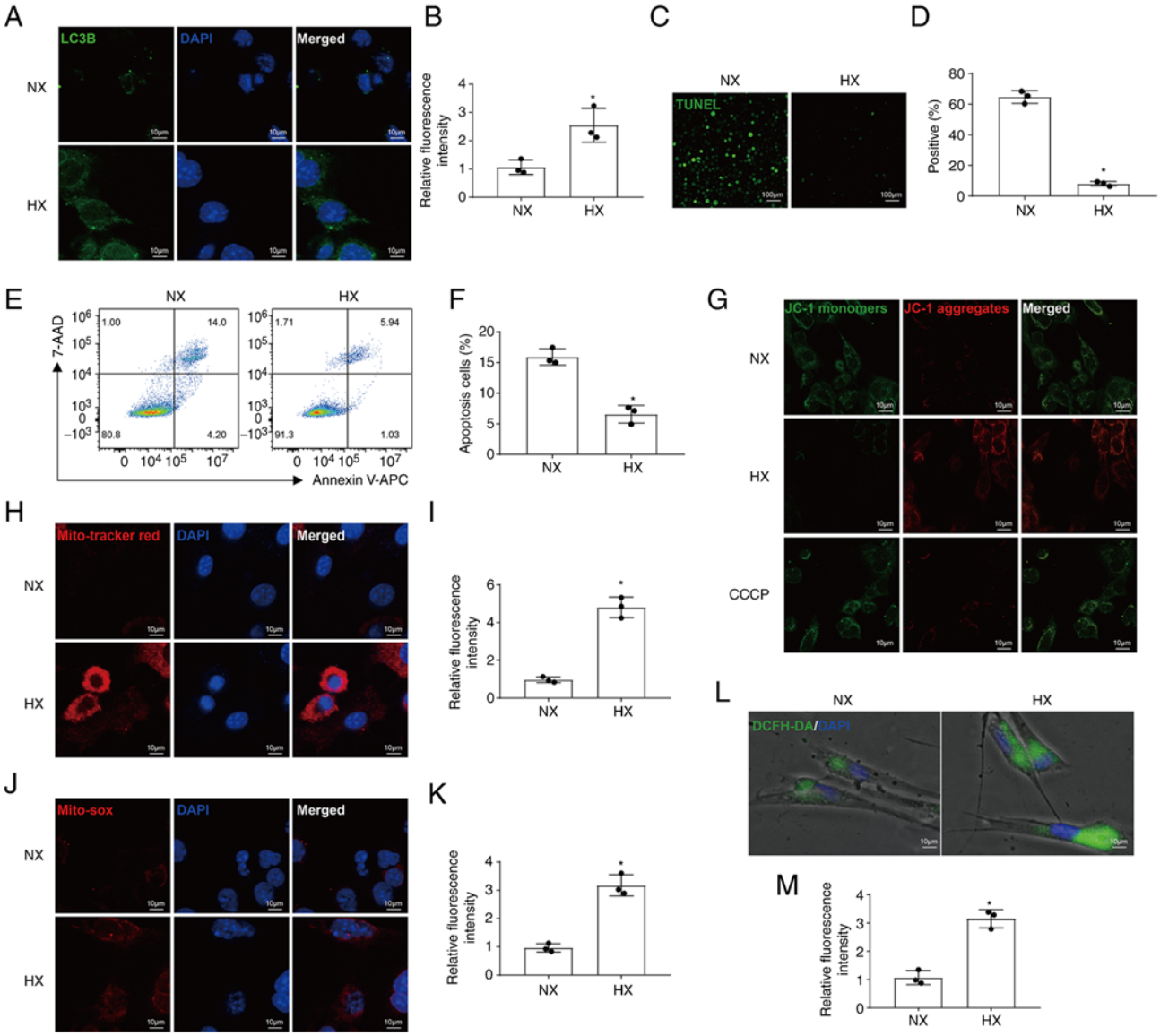

Figure 2. Hypoxia regulates mitophagy and apoptosis in chondrocytes. (A and B) IF images and quantification of LC3B expression (magnification, x400). (C and D) Representative IF images and quantification of TUNEL staining (magnification, x40). (E and F) Apoptosis was analyzed using the Annexin-APC/7-AAD kit and measured using FCM. (G) MMP was measured by IF using the JC-1 dye (magnification, x400). CCCP was used as a positive control. (H and I) Representative IF images and quantitative analysis of MitoTracker Red staining (magnification, x400). (J and K) Representative IF images and quantification of MitoSOX (magnification, x400). (L and M) Representative IF images and quantitative analysis of DCFH-DA (magnification, x400). *P<0.05 vs. NX. NX, normoxia; HX, hypoxia; FCM, flow cytometry; CCCP, carbonyl cyanide 3-chlorophenylhydrazone; IF, immunofluorescence.

The CRISPRa system effectively activates UCHL1. Next, the CRISPRa module was used to activate UCHL1 expression. BV was designed to express the CRISPRa module, which expressed sgRNA under the human U6 promoter and dCas9-VPR under the rat EF-1α promoter (Fig. 4A). dCas9 is derived from *Staphylococcus aureus* (Sa) and has a protospacer-adjacent motif (PAM, NNGRRT). Bac-Sa-UCHL1 expressed the Sa-dCas9-VPR and its associated sgRNA. As a control, Bac-Sa-con that expressed Sa-dCas9-VPR but not sgRNA was constructed (Fig. 4A). Chondrocytes were transduced with Bac-Sa-con or Bac-Sa-UCHL1 (designated as Sa-con and Sa-UCHL1 groups, respectively). UCHL1 expression was analyzed by RT-qPCR at 3, 5, 7, and 14 dpt. Compared with the Sa-con group, Sa-UCHL1 triggered significant UCHL1 upregulation for 7 days (Fig. 4B), suggesting that the CRISPRa system activated UCHL1 expression for at least 7 days. The expression levels of HIF-1α were increased in the Sa-UCHL1 group (Fig. 4C and D), while the intracellular ROS levels remained unchanged (Fig. 4E and F), indicating that endogenous activation of UCHL1 could induce the expression of HIF-1α without affecting intracellular ROS levels.

UCHL1 accelerates mitophagy, maintains mitochondrial function, and inhibits apoptosis. Next, the effects of endogenous activation of UCHL1 on mitophagy, mitochondrial function, and apoptosis were studied. The protein levels of LC3B were increased in the Sp-UCHL1 group (Fig. 5A and B), indicating the occurrence of intensive mitophagy. The proportion of apoptotic cells was reduced in the Sa-UCHL1 group, as measured by the TUNEL assay and FCM (Fig. 5C-F). IF images of cells stained with MitoTracker Red and JC-1 dyes revealed that the MMP

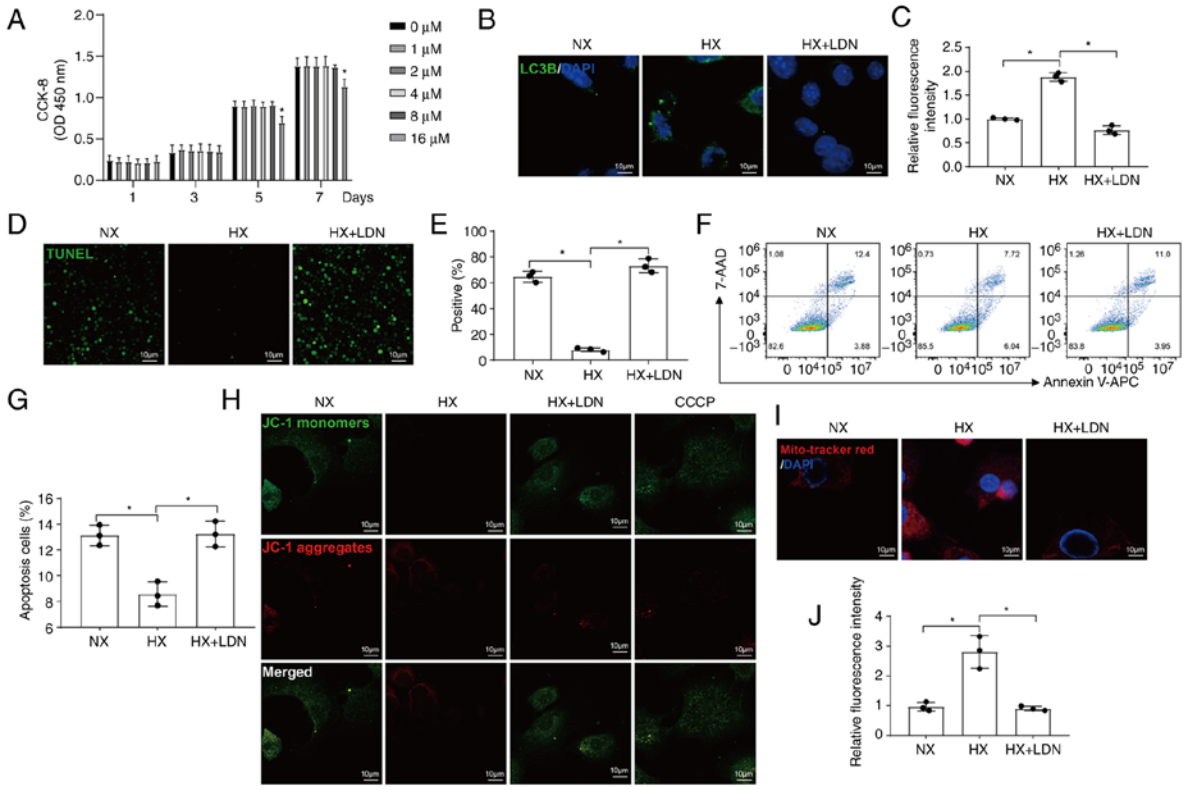

Figure 3. UCHL1 mediates the mitophagy regulated by hypoxia in chondrocytes. (A) CCK-8 assays of LDN-treated cells at the indicated concentrations. (B and C) Representative IF images and quantitative analysis of LC3B (magnification, x400). (D and E) Representative IF images and quantitative analysis of the TUNEL staining (magnification, x40). (F and G) Cell apoptosis analyzed using the Annexin-APC/7-AAD kit was measured by FCM. (H) The MMP was measured by IF using a JC-1 dye. CCCP was used as the positive control (magnification, x400). (I and J) Representative IF images and quantitative analysis of MitoTracker Red staining (magnification, x400). *P<0.05 vs. 0 μM. NX, normoxia; HX, hypoxia; UCHL1, Ubiquitin C-terminal hydrolase-L1; FCM, flow cytometry; CCCP, carbonyl cyanide 3-chlorophenylhydrazone; IF, immunofluorescence; LDN, LDN-57444.

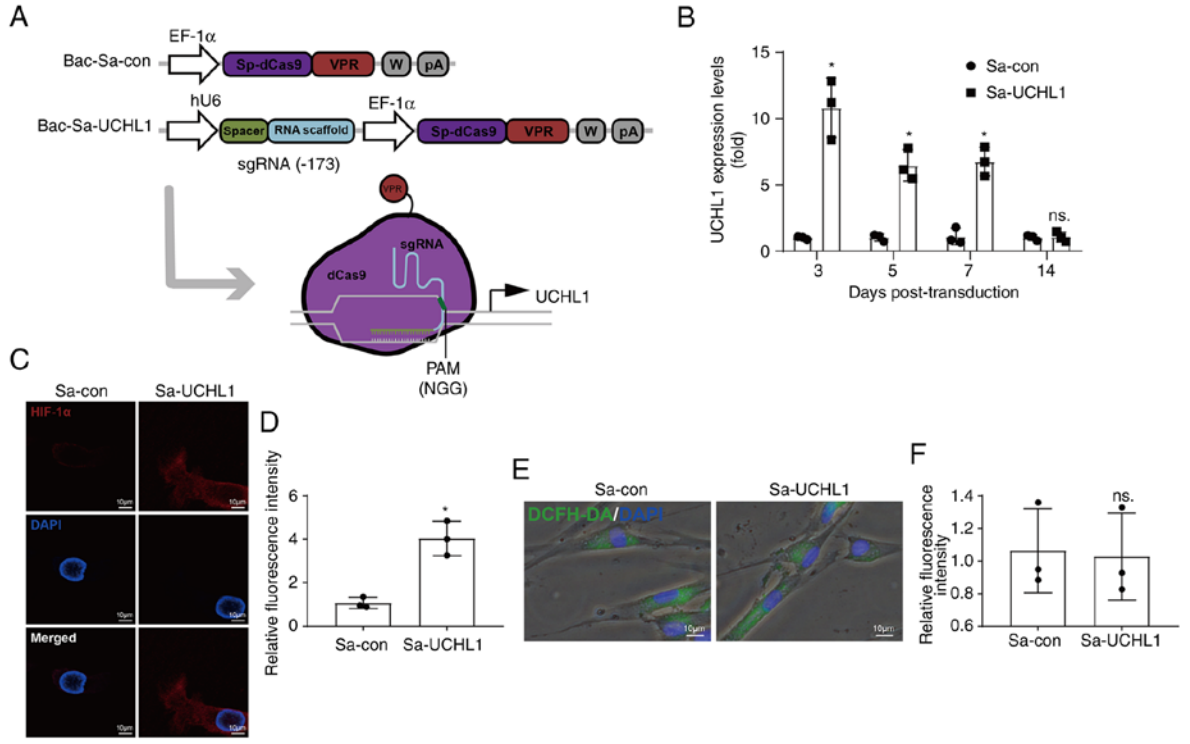

Figure 4. CRISPRa effectively activates UCHL1 upregulation. (A) Schematic illustration of Bac-Sa-con and Bac-Sa-UCHL1. The number mentioned after the gRNA represents the position relative to the transcription start site. (B) mRNA expression of UCHL1 after activation by the CRISPRa system. (C and D) Representative images and quantitative analysis of HIF-1α using IF staining (magnification, x400). (E and F) Representative IF images and quantitative analysis following DCFH-DA staining (magnification, x400). *P<0.05 vs. Sa-con. W, WPRE sequence. pA, polyadenylation signal; UCHL1, Ubiquitin C-terminal hydrolase-L1; Sa, *Staphylococcus aureus*; Sp, *Streptococcus pyogenes*; DCFH-DA, dichloro-dihydro-fluorescein diacetate; IF, immunofluorescence.

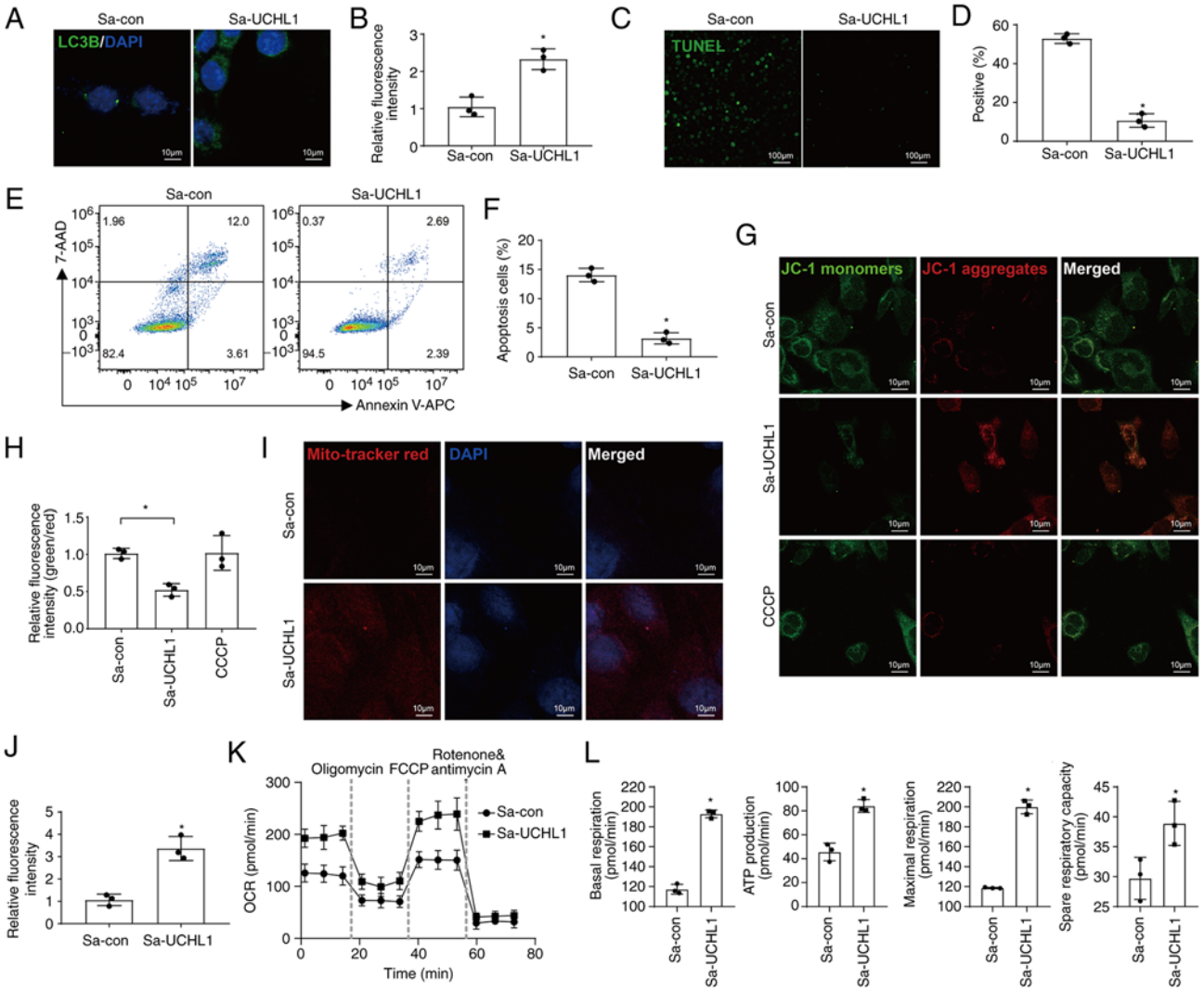

Figure 5. UCHL1 accelerates mitophagy, maintains mitochondrial function, and inhibits apoptosis. (A and B) IF images and quantification of LC3B expression (magnification, x400). (C and D) Representative IF images and quantification of TUNEL staining (magnification, x40). (E and F) Apoptosis was analyzed using the Annexin-APC/7-AAD kit and assessed using FCM. (G and H) MMP was measured by IF using JC-1 dye (magnification, x400). CCCP was used as a positive control. (I and J) Representative IF images and quantitative analysis of MitoTracker Red staining (magnification, x400). (K) OCR of chondrocytes following activation of UCHL1 using the CRISPRa system. (L) Effects of UCHL1 activated by CRISPRa on basal respiration, ATP production, maximal respiration, and spare respiratory capacity estimated using the OCR assay are shown. *P<0.05 vs. Sa-con. UCHL1, Ubiquitin C-terminal hydrolase-L1; Sa, *Staphylococcus aureus*; CCCP, carbonyl cyanide 3-chlorophenylhydrazone; IF, immunofluorescence; OCR, oxygen consumption rate; FCCP, fluoromethoxy carbonyl cyanide phenylhydrazone.

increased in the Sa-UCHL1 group (Fig. 5G-J). To investigate the mechanism by which endogenous activation of UCHL1 orchestrated mitochondrial function, the OCR of chondrocytes was measured according to the manufacturer's instructions. The results revealed that the OCR in chondrocytes was enhanced by the endogenous activation of UCHL1 (Fig. 5K). Specifically, UCHL1 increased basal respiration, ATP production, maximal respiration, and spare-respiratory capacity to maintain mitochondrial functions (Fig. 5L).

HIF-1α mediates mitochondrial functions modulated by UCHL1. To determine whether the effect of UCHL1 on mitophagy is dependent on HIF-1α, a specific inhibitor of HIF-1α, KC7F2, was used to ascertain the mechanism of action of UCHL1 in mitophagy. As shown in Fig. 6A, the expression of LC3B was increased by UCHL1 in chondrocytes. However, the augmented LC3B expression was inhibited by treatment with KC7F2 (Fig. 6A and B). The reduced ratio of apoptosis in chondrocytes via activation of UCHL1 was augmented by treatment with KC7F2 (Fig. 6C and D). OCR data indicated that chondrocytes displayed a higher OCR of cellular metabolism due to the activation of UCHL1. However, this increase in OCR was inhibited by treatment with FC7F2 (Fig. 6E). These results showed that HIF-1α mediated mitochondrial functions modulated by UCHL1.

Mitophagy mediates the inhibition of apoptosis by UCHL1. To examine the correlation between autophagy and apoptosis, cells in both the normoxia and hypoxia groups were subjected to treatment with 3-MA. The inhibition of mitophagy by 3-MA resulted in the cessation of LC3B accumulation induced by hypoxia (Fig. 7A and B). Additionally, the inhibition of mitophagy eliminated the hypoxia-induced increase in MMP (Fig. 7C-E) and suppressed apoptosis (Fig. 7F-I). These

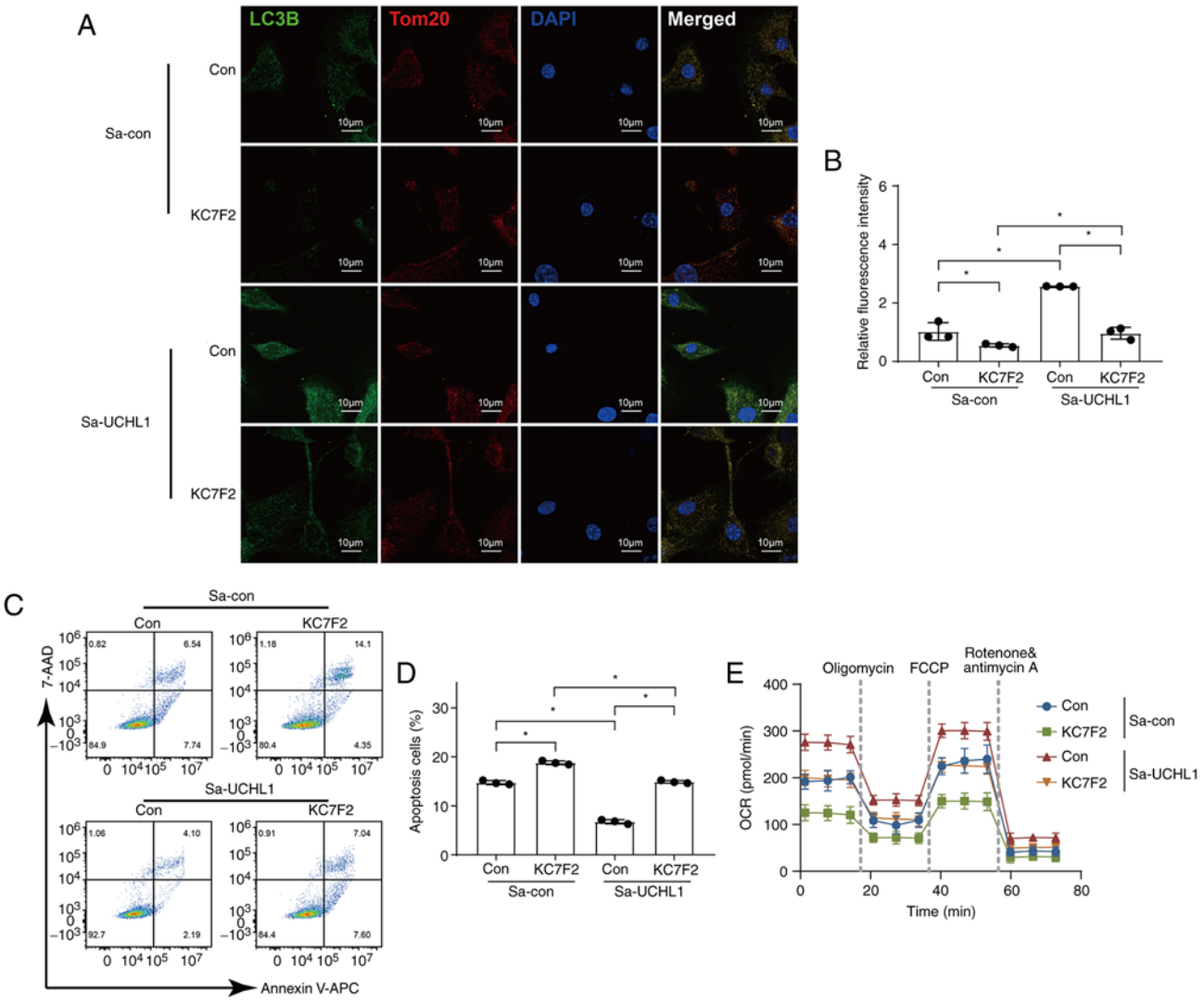

Figure 6. HIF-1α mediates the mitochondrial function modulated by UCHL1. (A and B) Representative IF double-staining images and quantitative analysis of LC3B and Tom20 in chondrocytes (magnification, x400). (C and D) Apoptosis was analyzed using the Annexin-APC/7-AAD kit and measured by FCM. (E) OCR of chondrocytes following activation of UCHL1 by the CRISPRa system and treatment with KC7F2, a HIF-1α inhibitor. *P<0.05. HIF-1α, hypoxia-inducible factor 1α; IF, immunofluorescence; OCR, oxygen consumption rate; FCM, flow cytometry; FCCP, fluoromethoxy carbonyl cyanide phenylhydrazone.

observations signify that the inhibition of apoptosis is contingent upon enhanced mitophagy.

Discussion

ADSCs have been widely used to treat diabetic foot disease (33), knee osteoarthritis (34), and cirrhosis (35) given their abundance, convenience of access, and low immunogenicity (36). A growing body of research has verified that ADSCs have significant potential in restoring the structure and functions of damaged tissues and may thus serve as novel treatment approaches for various refractory diseases such as cartilage defects (31). In the current study, it was found that UCHL1 expression was notably increased under hypoxic conditions in ADSC-derived chondrocytes. Given that UCHL1 abrogates VHL-mediated ubiquitination of HIF-1α (28) and that HIF-1α can alleviate apoptosis and senescence in chondrocytes through mitophagy (16), it was hypothesized that UCHL1 could alleviate apoptosis in chondrocytes via HIF-1α. Consistent with this hypothesis, the results of the current study suggested that UCHL1 attenuated apoptosis in chondrocytes derived from ADSCs via upregulation of HIF-1α-mediated mitophagy.

During mitophagy, cytosolic LC3B is recruited to the mitochondria, forming LC3B-positive puncta. The presence of LC3B puncta indicates the initiation of mitophagy (37). Moreover, efficient mitophagy helps maintain optimal MMP levels by facilitating the removal of damaged mitochondria, preventing their accumulation and associated metabolic defects (38). Therefore, LC3B and MMP were chosen as markers for mitophagy and detected in this study.

The response of chondrocytes to hypoxia-mediated by HIF-1α plays a vital role in regulating chondrogenesis by maintaining appropriate extracellular matrix production (39) and directing progenitor cell differentiation (21). In the present study, the *in vitro* experiments illustrated that hypoxia attenuated apoptosis and induced mitophagy, suggesting that hypoxia plays a role not only in regulating chondrogenesis, but also in cell survival. As hypoxia aids in the maintenance of chondral tissue, controlling the oxygen pressure may be an effective

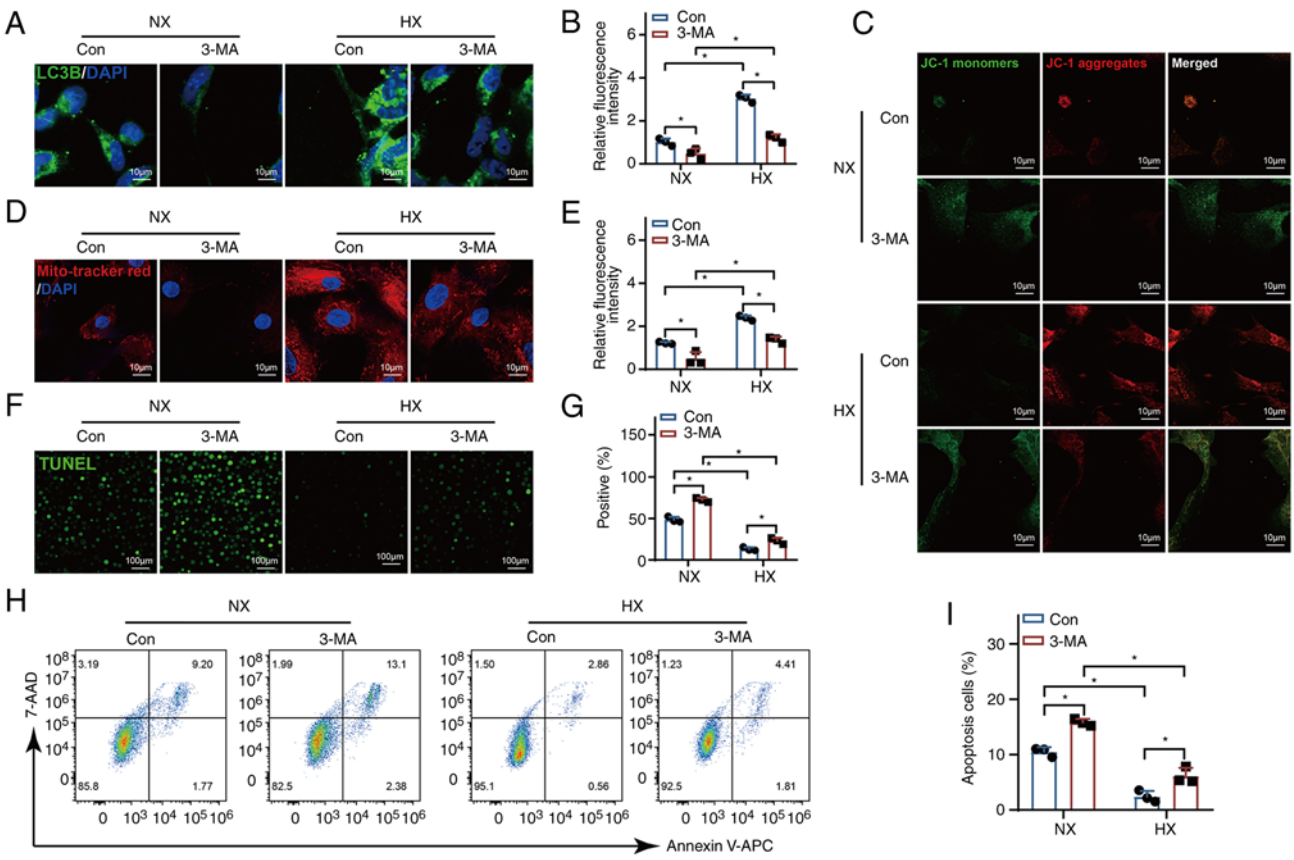

Figure 7. 3-MA inhibits autophagy and promotes apoptosis. (A and B) IF images and quantification of LC3B expression (magnification, x400). (C) MMP was measured by IF using the JC-1 dye (magnification, x400). (D and E) Representative IF images and quantitative analysis of MitoTracker Red staining (magnification, x400). (F and G) Representative IF images and quantification of TUNEL staining (magnification, x40). (H and I) Apoptosis was analyzed using the Annexin-APC/7-AAD kit and measured using FCM. *P<0.05. NX, normoxia; HX, hypoxia; IF, immunofluorescence; 3-MA, 3-Methyladenine.

strategy for engineering chondral tissues. However, hypoxia has been reported to cause oxidative stress and promote potentially undesirable effects on cell metabolism which may be detrimental to the formation of healthy chondral tissues (26). Consistent with these results, the results of the present study demonstrated that mitochondrial and intracellular ROS levels in chondrocytes were significantly increased under hypoxic conditions. Therefore, stabilization of HIF-1α under normoxic conditions has the potential to provide beneficial pro-chondrogenic effects of hypoxia in a potentially less deleterious and controlled manner.

Cofactors, such as p300 and the CREB-binding protein (CBP), are required to be recruited to the HIF transcriptional complex when HIF-1α binds to the Hypoxia response element in target gene promoters. The key residue present on HIF-1α that is involved in its binding with p300/CBP is asparagine-803 (Asn-803), which is also a target of 2-oxoglutarate (2-OG). As a factor inhibiting HIF-1α, 2-OG hydroxylates Asn-803 on HIF-1α, thereby preventing the binding of p300/CBP to HIF-1α, and in turn, disrupting the function of the HIF transcriptional complex (40-42). Certain compounds are reported to stabilize HIF-1α and enhance its binding through transcriptional cofactors under normoxic conditions. Among these compounds, dimethyloxalylglycine (DMOG) acts by competing with 2-OG by engaging the binding pocket of the prolyl hydroxylase active site (43). Recent research revealed that DMOG-loaded grafts promote vascular regeneration by stabilizing HIF-1α (44). Moreover, DMOG-doped zeolitic imidazolate frameworks-8 significantly promoted vascularized bone regeneration, primarily through the activation of HIF-1α (45). Nevertheless, although promising, DMOG lacks a high degree of specificity and may also target similarly structured enzymes that are essential for the formation of the collagen triple helix (46). In the present study, to stabilize HIF-1α under normoxic conditions in a controlled manner, endogenous UCHL1 was activated using the CRISPRa system. The results demonstrated that the intracellular ROS levels in chondrocytes were not increased following activation of UCHL1. Furthermore, UCHL1 accelerated mitophagy, maintained mitochondrial functions, and inhibited apoptosis by stabilizing HIF-1α.

In 1981, UCHL1 was initially described as a soluble nervous system-specific protein (47). Additional studies extended these observations by showing that UCHL1 was not only present in neurons of the central nervous system, but also in the heart (27), kidney (48), intervertebral disc (49), and periodontium (50). IF staining demonstrated that subcellular localization of UCHL1 is closely associated with the endoplasmic reticulum and mitochondria in neuroblastoma cells (51). Moreover, UCHL1 was shown to influence the morphology and respiratory functions of mitochondria in skeletal muscles, suggesting the existence of a link between UCHL1 and mitochondria of vital organelles (52). Recent reports suggest that UCHL1 can stabilize HIF-1α via abrogating ubiquitination of HIF-1α (27,28). Based

on these experiments, the role of UCHL1 on mitochondrial functions was assessed and it was found that UCHL1 induced mitophagy by abrogating the ubiquitination of HIF-1α in chondrocytes derived from ADSCs. In addition to regulating mitophagy, UCHL1 plays a role in mitochondrial dynamics and bioenergetics (53). Downregulation of UCHL1 reduces the levels of the mitochondrial fusion protein Mitofusin-2, resulting in mitochondrial enlargement and disruption of the tubular network in various cell lines (51). In addition, the respiratory function of the mitochondria was enhanced by the activation of UCHL1 in the present study. Thus, the effects of UCHL1 on mitochondria are multifaceted and require further investigation.

The CRISPRa system is an RNA-guided gene editing system repurposed from CRISPR-Cas9 and comprises gRNA and catalytically dead Cas9 (dCas9) (54). The gRNA was composed of a scaffold sequence responsible for dCas9 binding and a spacer sequence to recognize the target DNA. dCas9 is derived from mutated Cas9, the orthologs of which are derived from different bacteria such as *Streptococcus pyogenes* (SpCas9), *Staphylococcus aureus* (SaCas9), and *Neisseria meningitides* (NmCas9), among which SpCas9 is the most widely used (35). As the dCas9-VPR from *Staphylococcus aureus* (SadCas9-VPR) is more efficient than that from Streptococcus pyogenes in ADSCs (31), SadCas9-VPR was used in the present study. The SpdCas9 protein can be fused with a transcription activator (such as VP64) for CRISPRa of the target gene. In the present study, for more robust gene activation, SpdCas9 was fused with a tripartite activator, VPR, consisting of VP64, p65, and Rta to form SpdCas9-VPR to activate UCHL1, and the results demonstrated that UCHL1 expression was activated for at least 7 days. The size of SpdCas9-VPR is ~5.8 kb, which exceeds the packaging capacity of commonly used adeno-associated virus (55). Baculoviruses can deliver large amounts of genetic cargo (at least 38 kb) into ADSCs with an efficiency of >95%. As a non-pathogenic insect virus, baculoviruses neither replicate nor integrate their genome into the chromosomes of transduced cells, thereby minimizing their potential genotoxicity (31). Therefore, a baculovirus was employed to deliver the CRISPRa system to ADSCs in the current study.

Improving the safety profile of BV leads to short-term transgene expression, which is insufficient to maintain the long-term survival of ADSCs. The Cre/loxP-based hybrid BV system consists of a vector expressing Cre recombinase and another vector carrying a transgene cassette flanked by loxP sites, enabling the formation of DNA minicircles that can persist independent of chromosomes and prolong transgene expression (29). This is an area of ongoing research in our laboratory.

The present study investigated the impact of UCHL1 on chondrocytes, and shed light on its ability to prevent cell apoptosis via upregulation of HIF-1α-mediated mitophagy. By suppressing apoptosis, UCHL1 provides innate protection to chondrocytes and potentially contributes to sustaining cartilage integrity. This finding highlights novel avenues for cartilage tissue engineering by identifying UCHL1 as a molecular target for therapeutic interventions aimed at promoting cartilage repair. Additionally, the observed effects of UCHL1 on HIF-1α mediated mitophagy provide valuable insights into potential mechanisms for maintaining cellular homeostasis within cartilage tissues. These results not only contribute to our understanding of the underlying processes involved in cartilage health but also suggest a novel method for future cartilage repair. By harnessing the effect of UCHL1 and its ability to inhibit apoptosis and preserve mitochondrial function, researchers may develop innovative therapies to rejuvenate or regenerate damaged cartilage.

Acknowledgements

Not applicable.

Funding

This study was funded by the Science Research Cultivation Program of Stomatological Hospital, Southern Medical University (grant nos. PY2021028 and RC202202) and Guangzhou Basic and Applied Basic Research Foundation (grant no. 2023A04J0427).

Availability of data and materials

The datasets used and/or analyzed during the current study are available from the corresponding author on reasonable request.

Authors' contributions

QY contributed to the conception, design, data acquisition, analysis and interpretation, and drafting of the manuscript, and critically revised the manuscript. SS and YG contributed to the data acquisition and analysis, and drafted and critically revised the manuscript. SW and ML contributed to the data acquisition and critically revised the manuscript. ML contributed to the conception and design of the study. All authors have read and approved the final manuscript. ML and QY confirm the authenticity of all the raw data.

Ethics approval and consent to participate

Not applicable.

Patient consent for publication

Not applicable.

Competing interests

The authors declare that they have no competing interests.

References

1. Jiang Y and Tuan RS: Origin and function of cartilage stem/progenitor cells in osteoarthritis. Nat Rev Rheumatol 11: 206-212, 2015.
2. Vila PM, Jeanpierre LM, Rizzi CJ, Yaeger LH and Chi JJ: Comparison of autologous vs Homologous costal cartilage grafts in dorsal augmentation rhinoplasty: A systematic review and Meta-analysis. JAMA Otolaryngol Head Neck Surg 146: 347-354, 2020.
3. Zhang L, Wang JW, Ding J, Zhang X, Wang XM, Zhang ZZ and Yu RZ: A new technique for Asian nasal tip shaping: 'Twin tower' folding ear cartilage transplantation. Case Reports Plast Surg Hand Surg 9: 207-213, 2022.

4. Eftekhar N, Borjian A, Rafieian S, Borjian MA and Sahebi MA: Successful tracheal necrosis management using a pedicle pectoralis flap: A case report. Turk Gogus Kalp Damar Cerrahisi Derg 28: 547-551, 2020.
5. Calvert JW, Patel AC and Daniel RK: Reconstructive rhinoplasty: Operative revision of patients with previous autologous costal cartilage grafts. Plast Reconstr Surg 133: 1087-1096, 2014.
6. Wang S, Yang L, Cai B, Liu F, Hou Y, Zheng H, Cheng F, Zhang H, Wang L, Wang X, *et al*: Injectable hybrid inorganic nanoscaffold as rapid stem cell assembly template for cartilage repair. Natl Sci Rev 9: nwac037, 2022.
7. Johnson K, Zhu S, Tremblay MS, Payette JN, Wang J, Bouchez LC, Meeusen S, Althage A, Cho CY, Wu X and Schultz PG: A stem cell-based approach to cartilage repair. Science 336: 717-721, 2012.
8. Watanabe J, Yamada M, Niibe K, Zhang M, Kondo T, Ishibashi M and Egusa H: Preconditioning of bone marrow-derived mesenchymal stem cells with N-acetyl-L-cysteine enhances bone regeneration via reinforced resistance to oxidative stress. Biomaterials 185: 25-38, 2018.
9. Hughes CE, Coody TK, Jeong MY, Berg JA, Winge DR and Hughes AL: Cysteine Toxicity Drives Age-Related Mitochondrial Decline by Altering Iron Homeostasis. Cell 180: 296-310.e18, 2020.
10. He K, Nie L, Ali T, Liu Z, Li W, Gao R, Zhang Z, Liu J, Dai Z, Xie Y, *et al*: Adiponectin deficiency accelerates brain aging via mitochondria-associated neuroinflammation. Immun Ageing 20: 15, 2023.
11. Akter M, Ma H, Hasan M, Karim A, Zhu X, Zhang L and Li Y: Exogenous L-lactate administration in rat hippocampus increases expression of key regulators of mitochondrial biogenesis and antioxidant defense. Front Mol Neurosci Mar 16: 1117146, 2023.
12. Qu F, Wang P, Zhang K, Shi Y, Li Y, Li C, Lu J, Liu Q and Wang X: Manipulation of Mitophagy by 'All-in-One' nanosensitizer augments sonodynamic glioma therapy. Autophagy 16: 1413-1435, 2020.
13. Tang C, Han H, Yan M, Zhu S, Liu J, Liu Z, He L, Tan J, Liu Y, Liu H, *et al*: PINK1-PRKN/PARK2 pathway of mitophagy is activated to protect against renal ischemia-reperfusion injury. Autophagy 14: 880-897, 2018.
14. Kubli DA and Gustafsson ÅB: Mitochondria and mitophagy: The yin and yang of cell death control. Circ Res 111: 1208-1221, 2012.
15. Liu L, Zhang W, Liu T, Tan Y, Chen C, Zhao J, Geng H and Ma C: The physiological metabolite α-ketoglutarate ameliorates osteoarthritis by regulating mitophagy and oxidative stress. Redox Biol 62: 102663, 2023.
16. Hu S, Zhang C, Ni L, Huang C, Chen D, Shi K, Jin H, Zhang K, Li Y, Xie L, *et al*: Stabilization of HIF-1α alleviates osteoarthritis via enhancing mitophagy. Cell Death Dis 11: 481, 2020.
17. Wang FS, Kuo CW, Ko JY, Chen YS, Wang SY, Ke HJ, Kuo PC, Lee CH, Wu JC, Lu WB, *et al*: Irisin mitigates oxidative stress, chondrocyte dysfunction and osteoarthritis development through regulating mitochondrial integrity and autophagy. Antioxidants (Basel) 9: 810, 2020.
18. Taheem DK, Jell G and Gentleman E: Hypoxia inducible factor-1α in osteochondral tissue engineering. Tissue Eng Part B Rev 26: 105-115, 2020.
19. Li M, Ning J, Wang J, Yan Q, Zhao K and Jia X: SETD7 regulates chondrocyte differentiation and glycolysis via the Hippo signaling pathway and HIF-1α. Int J Mol Med 48: 210, 2021.
20. Xiaoshi J, Maoquan L, Jiwei W, Jinqiu N and Ke Z: SETD7 mediates the vascular invasion in articular cartilage and chondrocytes apoptosis in osteoarthriis. FASEB J 35: e21283, 2021.
21. Zhang H, Wang L, Cui J, Wang S, Han Y, Shao H, Wang C, Hu Y, Li X, Zhou Q, *et al*: Maintaining hypoxia environment of subchondral bone alleviates osteoarthritis progression. Sci Adv 9: eabo7868, 2023.
22. Lampert MA, Orogo AM, Najor RH, Hammerling BC, Leon LJ, Wang BJ, Kim T, Sussman MA and Gustafsson ÅB: BNIP3L/NIX and FUNDC1-mediated mitophagy is required for mitochondrial network remodeling during cardiac progenitor cell differentiation. Autophagy 15: 1182-1198, 2019.
23. Deng Z, Ou H, Ren F, Guan Y, Huan Y, Cai H and Sun B: LncRNA SNHG14 promotes OGD/R-induced neuron injury by inducing excessive mitophagy via miR-182-5p/BINP3 axis in HT22 mouse hippocampal neuronal cells. Biol Res 53: 38, 2020.
24. Ashammakhi N, Darabi MA, Kehr NS, Erdem A, Hu SK, Dokmeci MR, Nasr AS and Khademhosseini A: Advances in controlled oxygen generating biomaterials for tissue engineering and regenerative therapy. Biomacromolecules 21: 56-72, 2020.
25. Montesdeoca CYC, Stocco TD, Marciano FR, Webster TJ and Lobo AO: 3D bioprinting of smart oxygen-releasing cartilage scaffolds. J Funct Biomater 13: 252, 2022.
26. Majmundar AJ, Wong WJ and Simon MC: Hypoxia-inducible factors and the response to hypoxic stress. Mol Cell 40: 294-309, 2010.
27. Geng B, Wang X, Park KH, Lee KE, Kim J, Chen P, Zhou X, Tan T, Yang C, Zou X, *et al*: UCHL1 protects against ischemic heart injury via activating HIF-1α signal pathway. Redox Biol 52: 102295, 2022.
28. Goto Y, Zeng L, Yeom CJ, Zhu Y, Morinibu A, Shinomiya K, Kobayashi M, Hirota K, Itasaka S, Yoshimura M, *et al*: UCHL1 provides diagnostic and antimetastatic strategies due to its deubiquitinating effect on HIF-1α. Nat Commun 6: 6153, 2015.
29. Truong VA, Lin YH, Nguyen NTK, Hsu MN, Pham NN, Chang YH, Chang CW, Shen CC, Lee HS, Lai PL, *et al*: Bi-directional gene activation and repression promote ASC differentiation and enhance bone healing in osteoporotic rats. Mol Ther 30: 92-104, 2022.
30. Hsu MN, Yu FJ, Chang YH, Huang KL, Pham NN, Truong VA, Lin MW, Kieu Nguyen NT, Hwang SM and Hu YC: CRISPR interference-mediated noggin knockdown promotes BMP2-induced osteogenesis and calvarial bone healing. Biomaterials 252: 120094, 2020.
31. Nguyen NTK, Chang YH, Truong VA, Hsu MN, Pham NN, Chang CW, Wu YH, Chang YH, Li H and Hu YC: CRISPR activation of long non-coding RNA DANCR promotes bone regeneration. Biomaterials 275: 120965, 2021.
32. Livak KJ and Schmittgen TD: Analysis of relative gene expression data using real-time quantitative PCR and the 2(-Delta Delta C(T)) method. Methods 25: 402-408, 2001.
33. Moon KC, Suh HS, Kim KB, Han SK, Young KW, Lee JW and Kim MH: Potential of allogeneic adipose-derived stem cell-hydrogel complex for treating diabetic foot ulcers. Diabetes 68: 837-846, 2019.
34. Wiggers TG, Winters M, Van den Boom NA, Haisma HJ and Moen MH: Autologous stem cell therapy in knee osteoarthritis: A systematic review of randomised controlled trials. Br J Sports Med 55: 1161-1169, 2021.
35. Seki A, Sakai Y, Komura T, Nasti A, Yoshida K, Higashimoto M, Honda M, Usui S, Takamura M, Takamura T, *et al*: Adipose tissue-derived stem cells as a regenerative therapy for a mouse steatohepatitis-induced cirrhosis model. Hepatology 58: 1133-1142, 2013.
36. Qin Y, Ge G, Yang P, Wang L, Qiao Y, Pan G, Yang H, Bai J, Cui W and Geng D: An update on adipose-derived stem cells for regenerative medicine: Where challenge meets opportunity. Adv Sci (Weinh) 10: e2207334, 2013.
37. He G, Nie JJ, Liu X, Ding Z, Luo P, Liu Y, Zhang BW, Wang R, Liu X, Hai Y and Chen DF: Zinc oxide nanoparticles inhibit osteosarcoma metastasis by downregulating β-catenin via HIF-1α/BNIP3/LC3B-mediated mitophagy pathway. Bioact Mater 19: 690-702, 2022.
38. Onishi M, Yamano K, Sato M, Matsuda N and Okamoto K: Molecular mechanisms and physiological functions of mitophagy. EMBO J 40: e104705, 2021.
39. Stegen S, Laperre K, Eelen G, Rinaldi G, Fraisl P, Torrekens S, Van Looveren R, Loopmans S, Bultynck G, Vinckier S, *et al*: HIF-1α metabolically controls collagen synthesis and modification in chondrocytes. Nature 565: 511-515, 2019.
40. Sonoda K, Bogahawatta S, Katayama A, Ujike S, Kuroki S, Kitagawa N, Hirotsuru K, Suzuki N, Miyata T, Kawaguchi SI and Tsujita T: Prolyl Hydroxylase domain protein inhibitor not harboring a 2-Oxoglutarate scaffold protects against hypoxic stress. ACS Pharmacol Transl Sci 5: 362-372, 2022.
41. Usui-Ouchi A, Aguilar E, Murinello S, Prins M, Gantner ML, Wright PE, Berlow RB and Friedlander M: An allosteric peptide inhibitor of HIF-1α regulates hypoxia-induced retinal neovascularization. Proc Natl Acad Sci USA 117: 28297-28306, 2020.
42. Elvidge GP, Glenny L, Appelhoff RJ, Ratcliffe PJ, Ragoussis J and Gleadle JM: Concordant regulation of gene expression by hypoxia and 2-oxoglutarate-dependent dioxygenase inhibition: The role of HIF-1alpha, HIF-2alpha, and other pathways. J Biol Chem 281: 15215-15226, 2006.
43. Nguyen LK, Cavadas MA, Scholz CC, Fitzpatrick SF, Bruning U, Cummins EP, Tambuwala MM, Manresa MC, Kholodenko BN, Taylor CT and Cheong A: A dynamic model of the hypoxia-inducible factor 1α (HIF-1α) network. J Cell Sci 126: 1454-1463, 2013.

44. Rafique M, Wei T, Sun Q, Midgley AC, Huang Z, Wang T, Shafiq M, Zhi D, Si J, Yan H, *et al*: The effect of hypoxia-mimicking responses on improving the regeneration of artificial vascular grafts. Biomaterials 271: 120746, 2021.
45. Zhang X, Chen JY, Pei X, Li YH, Feng H, He ZH, Xie WJ, Pei XB, Zhu Z, Wan QB and Wang J: One-Pot facile encapsulation of dimethyloxallyl glycine by nanoscale zeolitic imidazolate frameworks-8 for enhancing vascularized bone regeneration. Adv Healthc Mater 12: e2202317, 2023.
46. Myllyharju J: Prolyl 4-hydroxylases, the key enzymes of collagen biosynthesis. Matrix Biol 22: 15-24, 2003.
47. Jackson P and Thompson RJ: The demonstration of new human brain-specific proteins by high-resolution two-dimensional polyacrylamide gel electrophoresis. J Neurol Sci 49: 429-438, 1981.
48. Hu Y, Qi C, Shi J, Tan W, Adiljan Abdurusul, Zhao Z, Xu Y, Wu H and Zhang Z: Podocyte-specific deletion of ubiquitin carboxyl-terminal hydrolase L1 causes podocyte injury by inducing endoplasmic reticulum stress. Cell Mol Life Sci 80: 106, 2023.
49. Zhu Z, He Z, Tang T, Wang F, Chen H, Li B, Chen G, Wang J, Tian W, Chen D, *et al*: Integrative bioinformatics analysis revealed mitochondrial dysfunction-related genes underlying intervertebral disc degeneration. Oxid Med Cell Longev 2022: 1372483, 2022.
50. Lin L, Li S, Hu S, Yu W, Jiang B, Mao C, Li G, Yang R, Miao X, Jin M, *et al*: UCHL1 impairs periodontal ligament stem cell osteogenesis in periodontitis. J Dent Res 102: 61-71, 2023.
51. Cerqueira FM, von Stockum S, Giacomello M, Goliand I, Kakimoto P, Marchesan E, De Stefani D, Kowaltowski AJ, Ziviani E and Shirihai OS: A new target for an old DUB: UCH-L1 regulates mitofusin-2 levels, altering mitochondrial morphology, function and calcium uptake. Redox Biol 37: 101676, 2020.
52. Gao H, Antony R, Srinivasan R, Wu P, Wang X and Li Y: UCHL1 regulates oxidative activity in skeletal muscle. PLoS One 15: e0241716, 2020.
53. Bouron A, Aubry L, Loreth D, Fauvarque MO and Meyer-Schwesinger C: Role of the deubiquitinating enzyme UCH-L1 in mitochondrial function. Front Cell Neurosci 17: 1149954, 2023.
54. Komor AC, Badran AH and Liu DR: CRISPR-Based technologies for the manipulation of eukaryotic genomes. Cell 168: 20-36, 2017.
55. Li C and Samulski RJ: Engineering adeno-associated virus vectors for gene therapy. Nat Rev Genet 21: 255-272, 2020.